innovative techniques

Near-infrared spiroximetry: noninvasive measurements of venous saturation in piglets and human subjects

MARIA ANGELA FRANCESCHINI,[1,2] DAVID A. BOAS,[2] ANNA ZOURABIAN,[2]
SOLOMON G. DIAMOND,[2] SHALINI NADGIR,[1] DAVID W. LIN,[1]
JOHN B. MOORE,[2] AND SERGIO FANTINI[1]
[1]*Bioengineering Center, Department of Electrical Engineering and Computer Science
Tufts University, Medford 02155-6013; and* [2]*NMR Center, Massachusetts General
Hospital, Harvard Medical School, Charlestown, Massachusetts 02129*

**Franceschini, Maria Angela, David A. Boas, Anna
Zourabian, Solomon G. Diamond, Shalini Nadgir,
David W. Lin, John B. Moore, and Sergio Fantini.** Near-
infrared spiroximetry: noninvasive measurements of venous
saturation in piglets and human subjects. *J Appl Physiol* 92:
372–384, 2002.—We present a noninvasive method to mea-
sure the venous oxygen saturation (Sv_{O_2}) in tissues using
near-infrared spectroscopy (NIRS). This method is based on
the respiration-induced oscillations of the near-infrared ab-
sorption in tissues, and we call it spiroximetry (the prefix
spiro means respiration). We have tested this method in
three piglets (hind leg) and in eight human subjects (vastus
medialis and vastus lateralis muscles). In the piglet study,
we compared our NIRS measurements of the Sv_{O_2} (Sv_{O_2}-
$NIRS_{resp}$) with the Sv_{O_2} of blood samples. Sv_{O_2}-$NIRS_{resp}$ and
Sv_{O_2} of blood samples agreed well over the whole range of
Sv_{O_2} considered (20–95%). The two measurements showed
an average difference of 1.0% and a standard deviation of the
difference of 5.8%. In the human study, we found a good
agreement between Sv_{O_2}-$NIRS_{resp}$ and the Sv_{O_2} values mea-
sured with the NIRS venous occlusion method. Finally, in a
preliminary test involving muscle exercise, Sv_{O_2}-$NIRS_{resp}$
showed an expected postexercise decrease from the initial
baseline value and a subsequent recovery to baseline.

tissue spectroscopy; frequency-domain; pulse oximetry; he-
moglobin saturation

THE POSSIBILITY OF USING LIGHT to measure the oxygen
saturation of hemoglobin in vivo has been explored
since the 1940s (37). The feasibility of optical blood
oximetry stems from the oxygenation dependence of
the optical spectrum of hemoglobin. This is illustrated
in Fig. 1, which shows the absorption spectra of 100
μM hemoglobin for oxygen saturation values of 0, 20,
40, 60, 80, and 100%. The spectra of Fig. 1 were
calculated from published values of the molar extinc-
tion coefficients of oxyhemoglobin (HbO_2) and deoxyhe-
moglobin (Hb) (43, 53).

Oxygen saturation of the pulmonary capillary blood
in rabbits has been measured by using dynamic inva-
sive techniques (48). Near-infrared light in the wave-
length range from 700 to 900 nm results in a sufficient
penetration depth for the noninvasive optical monitor-
ing of skeletal muscle, cerebral gray matter, and breast
tissue. As a result, near-infrared techniques allow a
noninvasive assessment of hemoglobin saturation for a
wide range of applications, such as the study of muscle
metabolism (7, 9, 12, 29, 45), the diagnosis of vascular
disorders (2, 20, 32, 33, 44, 49), functional brain imag-
ing (3, 10, 24, 30, 35, 50), and breast cancer detection
(23, 28, 40, 42, 46).

If near-infrared light is highly sensitive to the oxy-
gen saturation of hemoglobin, then its large penetra-
tion depth inside tissues implies that the arterial,
venous, and capillary compartments all contribute to
the optical signal. The average hemoglobin oxygen-
ation measured with near-infrared spectroscopy (NIRS)
(19, 34, 41) is usually referred to as tissue oxygen
saturation (St_{O_2}). St_{O_2} values are assumed to be in
between arterial and local venous saturation values
(Sa_{O_2} and Sv_{O_2}, respectively). A number of research
studies have investigated the relationship between the
near-infrared (noninvasive) measurement of St_{O_2} and
the values of Sa_{O_2} and local Sv_{O_2} measured invasively
from drawn blood samples (31, 51). The contribution of
the arterial compartment to the noninvasive optical
signal can be isolated because of its unique temporal
dynamics associated with the systolic-diastolic blood
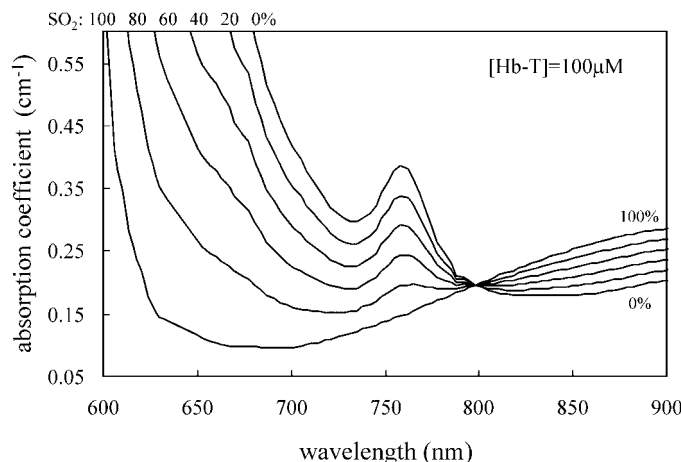pressure variation at the heartbeat frequency (1). The

---

Fig. 1. Near-infrared absorption spectra of 100 μM hemoglobin concentration ([Hb-T], where T stands for total) for different values of the oxygen saturation (S_{O_2}) in the range of 0–100%. The curve for $S_{O_2} = 0\%$ corresponds to the deoxyhemoglobin (Hb) absorption spectrum, whereas the curve for $S_{O_2} = 100\%$ corresponds to the oxyhemoglobin (HbO_2) absorption spectrum. These spectra have been computed from published spectra of the molar extinction coefficients of HbO_2 and Hb (43, 53).

pulsatile component of the optical signals at two or more wavelengths at the heartbeat frequency is used by conventional (1, 36) or self-calibrated (21) pulse oximeters to measure the Sa_{O_2}. Sa_{O_2} is a parameter that provides information about the ventilation and the oxygen exchange in the lungs. In contrast, Sv_{O_2} is a parameter that reflects the local balance between blood flow and oxygen consumption. The noninvasive optical measurement of Sv_{O_2} is complicated by the fact that the isolation of the contribution of the venous compartment to the noninvasive optical signal is not straightforward. There are no clinical devices presently capable of monitoring Sv_{O_2} noninvasively.

A number of experimental approaches have been proposed to measure Sv_{O_2} from induced local changes in the venous blood volume. For instance, proposed approaches involve a venous occlusion in a limb (13, 39, 55, 56), tilting the patient's head down by 15 degrees (47), a partial jugular vein occlusion (15, 54), or mechanical ventilation (52). In all these approaches, Sv_{O_2} is optically measured as the ratio between the increases in the HbO_2 concentration ([HbO_2]) and the total hemoglobin concentration (equal to [HbO_2] + [Hb], where [Hb] is deoxyhemoglobin concentration) induced by the local increase in venous blood volume. To overcome the limitations of these methods, which can either be applied only to the limbs (venous occlusion method) or require an external perturbation (partial jugular vein occlusion, mechanical ventilation, and tilting methods), we propose an alternative approach that is an extension of the method of Wolf et al. (52). This approach involves no external perturbations and is applicable to subjects who are breathing either spontaneously or synchronously with a metronome set at their average respiratory frequency. Furthermore, this method can provide continuous and real-time monitoring of Sv_{O_2}. The basic idea is to measure Sv_{O_2} from the amplitude of the optically measured [HbO_2] and [Hb] oscillations at the respiratory frequency. The basic hypothesis, originally formulated in this context and tested on the brain of mechanically ventilated infants by Wolf et al., is that the oscillatory components of [HbO_2] and [Hb] at the breathing rate are mostly representative of the venous compartment. Because the venous compliance is ~20 times as large as the arterial compliance (4), a given change in the blood pressure in the veins causes a venous volume change ~20 times as large as the arterial volume change corresponding to the same pressure change in the arteries. During normal breathing, the inspiration phase involves a decrease in the intrathoracic pressure and an increased pressure gradient between the peripheral venous system and the intrathoracic veins. This causes blood to be drawn from the extrathoracic veins into the intrathoracic vessels and heart (26). Because of the vein valves, venous return is increased more by inspiration than it is decreased by expiration (38). The net effect is the so-called respiratory pump that facilitates the venous return from the periphery by the respiration-induced periodic fluctuations in the central venous pressure (38). As a result of the respiratory pump, the peripheral venous blood volume oscillates at the respiratory frequency, decreasing during inspiration and increasing during expiration.

It is on this oscillatory component at the respiratory frequency that we base our near-infrared measurement of the Sv_{O_2}. We coin the term spiroximeter to indicate an instrument for measuring the Sv_{O_2} from respiration-induced oscillations in the venous blood pressure and in the venous volume fraction in tissues. It must be observed that respiration may also induce perturbations to the heart rate (respiratory sinus arrhythmia) and consequently to the cardiac output and arterial blood pressure. As a result, the arterial compartment volume may, in general, also oscillate at the respiratory frequency; thus near-infrared spiroximetry data must be carefully examined to guarantee a reliable reading of Sv_{O_2}.

We report a validation study conducted on the hind leg of three piglets, in which we compared the near-infrared measurements of Sv_{O_2} (Sv_{O_2}-NIRS) with the Sv_{O_2} values obtained by the gas analysis of venous blood samples (Sv_{O_2}-blood). To show the applicability of spiroximetry to human subjects, we also conducted a preliminary test on the vastus medialis and vastus lateralis muscles of healthy volunteers at rest and postexercise.

MATERIALS AND METHODS

Tissue spectrometer. The near-infrared measurements were performed with a frequency-domain tissue spectrometer (model 96208, ISS, Champaign, IL) (18, 25). This instrument uses two parallel photomultiplier tube detectors that are time shared by eight multiplexed laser diodes emitting at 636, 675, 691, 752, 780, 788, 830, and 840 nm, respectively. The frequency of intensity modulation is 110 MHz, and heterodyne detection is performed with a cross-correlation frequency of 5 kHz. The multiplexing rate, i.e., the frequency

of sequential laser switching, is 100 Hz. As a result, 50 cross-correlation periods are acquired during the on time of each laser diode, and a complete acquisition cycle over the eight wavelengths is completed every 80 ms. The laser diodes and the photomultiplier tubes are all coupled to fiber optics. The eight individual illumination fibers, each 400 μm in internal diameter, are arranged into a fiber bundle having a rectangular cross-section of 3.5×2.0 mm^2. The collecting circular fiber bundles are 3.0 mm in internal diameter. The optical fibers are placed in contact with the skin by means of a flexible plastic probe. The optical probe arranges the tips of the illuminating and collecting fiber bundles along a line, with the two collecting fiber bundles at distances of 1.0 and 2.0 cm from the single illuminating bundle. In some cases, we have used a second tissue spectrometer to perform simultaneous measurements on both legs (*piglets 2* and *3*) or at different locations on the same leg (human subjects). In the second tissue spectrometer (which used the optical *probes PL* and *HVL* defined below), the 840-nm laser diode was replaced by a laser diode emitting at 814 nm.

Measurements on piglets. We performed measurements on three piglets that were 15 ± 1 days old and weighed 5 ± 1 kg. The experimental arrangement for the piglet measurements is schematically illustrated in Fig. 2. The piglets were anesthetized by inhalation of 3–4% isoflurane administered by means of a breathing mask applied to the piglet's snout. The animals were not mechanically ventilated, and they breathed freely throughout the experiment. A strain-gauge belt (Sleepmate/Newlife Technologies, Resp-EZ) was placed around the piglet's thorax to continuously monitor the respiratory excursion. A pulse oximeter (Nellcor, N-200) continuously recorded the heart rate at the foot of the right hind leg. The analog outputs from the strain gauge and the pulse oximeter were fed to the auxiliary input ports of the tissue spectrometer for continuous coregistration of optical and physiological data. A femoral cutdown was performed into the left inferior femoral vein to insert a catheter for periodic blood sampling. The femoral venous blood samples were run through a commercial blood-gas analyzer (Instrumentation Laboratory, model 1304 pH/blood-gas analyzer) to obtain invasive readings of Sv$_{O_2}$-blood. One optical probe (identified as *probe PR*) was always located on the right (noncatheterized) hind leg. In *piglets 2* and *3*, a second probe (*probe PL*) was placed on the catheterized (left) leg. The protocol consisted of varying the femoral Sv$_{O_2}$ over the approximate range of 20–95% by modulating the volume fraction of oxygen inspired by the piglet (F$_{I_{O_2}}$) over the range of 10–100%. The oxygenation cycles performed on the three piglets are illustrated in Fig. 3. Each cycle consisted of varying the F$_{I_{O_2}}$ approximately every 4–6 min through the values of ~40, 15, 10, and 100% (*piglets 1* and *2*) or ~40, 20, 17.5, 15, 12.5, 10, and 100% (*piglet 3*). We performed two F$_{I_{O_2}}$ cycles on *piglet 1*, four on *piglet 2*, and three on *piglet 3*. For each specific value of F$_{I_{O_2}}$, we acquired about 3,000 optical data points [4 min $\times$ (60 s/min)/(80 ms/data point)] or more. During *cycles C* and *D* on *piglet 2*, the optical *probe PR* was slightly moved with respect to the location examined during *cycles A* and *B*, to collect data on two different muscle volumes during the two cycle pairs *A-B* and *C-D*. Optical *probe PR* always collected data on the right hind leg, whereas *probe PL* was placed on the left hind leg during *cycles A* and *B* of *piglet 2* and *cycles A* and *B* of *piglet 3* (we did not collect data with the optical *probe PL* on *piglet 1*, during *cycles C-D* on *piglet 2*, and during *cycle C* on *piglet 3*). In all three piglets, the invasive measurement of Sv$_{O_2}$ from a femoral vein blood sample was performed at the end of each F$_{I_{O_2}}$ interval, as shown in Fig. 3. Motion artifacts were minimized in the optical data by securing the piglet's legs to the operating table. The protocol was approved by the Institutional Review Board of the Massachusetts General Hospital, where the piglet experiments were performed.

Measurements on human subjects. We performed measurements on eight healthy human subjects (6 men and 2 women; mean age of 24.5 yr, age range of 20–35 yr). The subjects sat on a comfortable chair and rested for 10–15 min before the experimental protocol was started. A pneumatic cuff was placed around the right thigh of the subject to later induce a venous occlusion by inflating the cuff to a pressure of 70 mmHg. A pulse oximeter probe (Nellcor, N-200) was placed
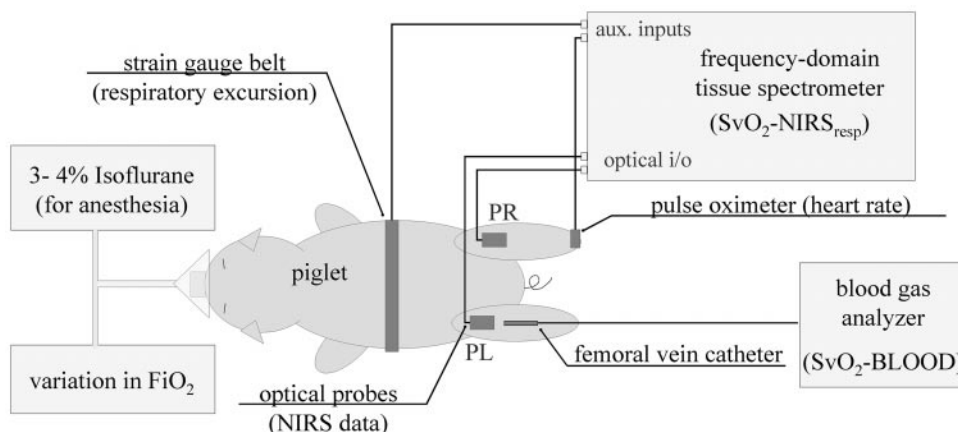

Fig. 2. Experimental arrangement for the piglet study. A breathing mask applied to the piglet's snout provided the 3–4% isoflurane anesthetic and was connected to the oxygen line for variations in the fraction of inspired oxygen (F$_{I_{O_2}}$). A strain-gauge belt and a pulse oximeter monitored the respiratory excursion and the heart rate, respectively, and their analog outputs were directed to the auxiliary inputs of the frequency-domain tissue spectrometer (ISS, Champaign, IL, model 96208). One or two optical probes (PR on the right hind leg and PL on the left hind leg) of the tissue spectrometer were used to measure the near-infrared tissue absorption with a time resolution of 80 ms. The absorption oscillations at the respiratory frequency were processed to provide measurement of the venous O$_2$ saturation (Sv$_{O_2}$-NIRS$_{resp}$) (NIRS is near-infrared spectroscopy). Invasive measurements of the venous O$_2$ saturation (designated Sv$_{O_2}$-blood) were obtained by gas analysis of venous blood samples collected by a femoral vein catheter. aux, Auxiliary; optical I/O, optical input/output.
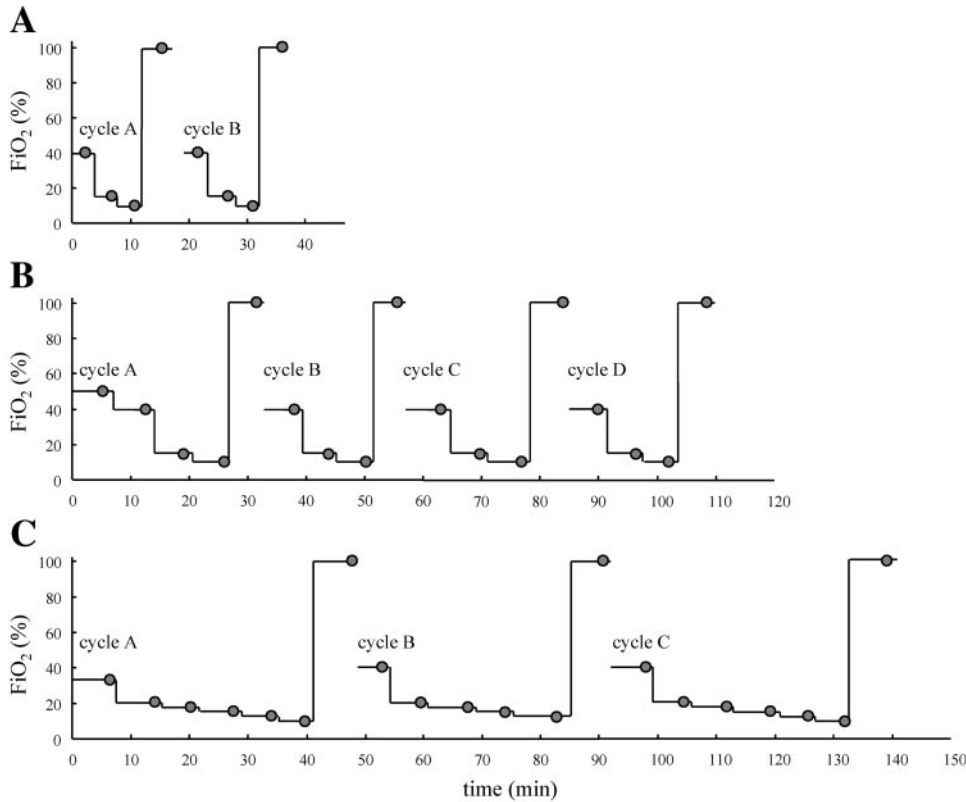
Fig. 3. Schematic representation of FI_{O_2} cycles for *piglet 1* (*A*), *piglet 2* (*B*), and *piglet 3* (*C*). ●, Time at which venous blood samples were run through the blood-gas analyzer for Sv_{O_2}-blood measurements.

on the index finger of the left hand. A strain-gauge belt (Sleepmate/Newlife Technologies, Resp-EZ) was placed around the subject's upper abdomen to monitor the respiratory excursion. As in the piglet experiment, we used the analog outputs of the pulse oximeter and strain gauge for continuous coregistration of the physiological and near-infrared data. Two optical probes were placed on the right thigh; the first probe (*probe HVM*) was positioned on top of a visible superficial vein of the vastus medialis muscle, and the second probe (*probe HVL*) was placed on the vastus lateralis muscle, far from visible superficial veins. During the measurements, we asked the subject to breathe regularly, following a metronome whose frequency was set to the average breathing rate of the subject at rest (typically 14–15 breaths/min). During the whole experiment, the subject was asked to breathe at the same frequency as the metronome pace. No subjects experienced any discomfort or difficulties with this procedure. The measurement protocol consisted of 2 min of baseline (we acquired 1,535 optical data points at 80 ms/point), followed by 40 s of venous occlusion, and a final recovery period of a few minutes. A few subjects performed an additional exercise routine to test the effect of exercise on the measured value of Sv_{O_2}-NIRS$_{\text{resp}}$ on the muscle. The exercise consisted of raising the right foot, voluntarily contracting the leg muscles (isometric contraction), until the subject felt tired. The human study was approved by the Institutional Review Board of Tufts University, where the human experiments were performed; all subjects gave their written, informed consent.

Near-infrared data processing for the measurement of Sv_{O_2}. We used a modified Beer-Lambert law approach (14) to translate the temporal intensity ratio collected at each wavelength [$I(\lambda, t)/I(\lambda, 0)$, where I is intensity, λ is wavelength, and t is time] at a distance of 1.0 cm from the illumination point, into a time variation in the tissue absorption [$\Delta\mu_a(\lambda, t)$,

where μ_a is the tissue absorption coefficient]. This approach was implemented by applying the following equation (14)

$$\Delta\mu_a(\lambda,t) = \frac{1}{L_{\text{eff}}} \ln\left[\frac{I(\lambda,0)}{I(\lambda,t)}\right] \quad (1)$$

where L_{eff} is the effective optical pathlength from the illuminating point to the light collection point. We measured L_{eff} by quantifying μ_a and the reduced scattering coefficient (μ_s') using the frequency-domain multidistance method (17). The diffusion-theory relationship that gives L_{eff} in terms of μ_a, μ_s', and the source-detector separation (r) in a semi-infinite turbid medium (where the illumination and collection points are at the boundary of the turbid medium) is the following (17)

$$L_{\text{eff}} = \frac{3\mu_s' r^2}{2(r\sqrt{3\mu_a\mu_s'} + 1)} \quad (2)$$

More details on this hybrid frequency-domain [to measure $L_{\text{eff}}(\lambda)$] and continuous wave (modified Beer-Lambert law) approach are given in Refs. 14, 17, 21, and 22. *Equation 2* shows that for typical values of the near-infrared μ_a and μ_s', say $\mu_a = 0.1$ cm^{-1} and $\mu_s' = 10$ cm^{-1}, the value of L_{eff} is ~5.5 cm for $r = 1$ cm. The multi-distance scheme was implemented by considering the data collected by the two fiber bundles located at two different distances (1.0 and 2.0 cm) from the source fiber bundle. At these source detector distances, the diffusion regime of light propagation in tissues is already established (18). As an alternative to the diffusion equation model to describe the spatial dependence of the optical signal, empirical approaches have been proposed (6). The different sensitivity of the two detector channels was accounted for by a preliminary calibration measurement on a synthetic tissue-like sample. The applicability of the initial calibration to the

whole data set was verified at the end of each measurement session by repositioning the optical probe on the calibration sample. We typically reproduced the calibration values of the block optical coefficients to within 10%. In the piglet experiments, we updated the measured values of L_{eff} at each wavelength every time the $F_{I_{O_2}}$ was changed. Specifically, L_{eff} was computed, according to *Eq. 2*, from average measurements of μ_a and μ_s' over the last 80 s of each period corresponding to a specific $F_{I_{O_2}}$ value. For the measurements on human subjects, we computed an initial value of L_{eff} (at each wavelength) over the first 2 min of baseline, and we used this value for the analysis of the data over the whole measurement session. The long integration time for the mean pathlength measurements (80 s in the piglet experiment, 120 s in the human subjects measurements) realized a low-pass filter that minimized the time-varying contributions from the Hb oscillations caused by the arterial pulsation and breathing. Furthermore, the two-distance measurement scheme for the mean pathlength measurement also provided some level of spatial averaging. In contrast, the optical data for the measurement of Sv_{O_2} were acquired with an 80-ms temporal resolution and with the use of a single source-detector distance (1 cm).

To measure the Sv_{O_2}, we followed a two-step procedure. First, we computed the amplitude of the absorption oscillations at the respiratory frequency at each of the eight wavelengths considered. Second, we fit the spectrum of the experimental absorption amplitude with the hemoglobin absorption spectrum. We have used two alternative methods to quantify the absorption oscillations at the respiratory frequency. The first method is based on the fast Fourier transform (FFT) of $\Delta\mu_a(t)$. The sum of the amplitudes of the FFT of $\Delta\mu_a$ over the respiratory frequency band yields a measure of the amplitude of the respiration-induced absorption oscillations. This method assumes that the Fourier spectrum of $\Delta\mu_a$ clearly shows a discernable peak at the respiratory frequency. The second method is based on a band-pass (BP) filter of $\Delta\mu_a(t)$ and on a modeling algorithm (MA) (sine-wave fit). The BP filter serves the purpose of isolating the absorption oscillations at the respiratory frequency by suppressing higher and lower frequency components in $\Delta\mu_a(t)$. The MA consists of fitting a sine wave to $\Delta\mu_a(BP)$ over each respiratory cycle. The amplitude of the fitted sine wave gives an estimate of the absorption oscillation amplitude at the respiratory frequency. As a result, the second method (BP + MA) achieves a reading of Sv_{O_2} from each individual respiration cycle, whereas the first method (FFT) requires multiple respiration cycles to produce a Sv_{O_2} reading. Both methods provide phase readings that can be used to verify that the respiration-induced absorption oscillations at different wavelengths are in phase with each other. We indicate the Sv_{O_2} measurement according to the FFT and BP + MA methods with Sv_{O_2}-$NIRS_{resp}$(FFT) and Sv_{O_2}-$NIRS_{resp}$(BP), respectively.

In the piglet experiments, we evaluated the FFT of $\Delta\mu_a$ over 256 data points, corresponding to a time trace of 20.5 s, to achieve reliable spectra from a number of breathing periods (typically 13–16). Furthermore, we averaged about 800 successive FFTs (each computed from a data set shifted by one data point with respect to the previous one), so that the total number of data points resulting in a single Sv_{O_2} reading was on the order of 1,000, corresponding to a train of data 80 s long. This 80-s-long data set was chosen to be at the end of each $F_{I_{O_2}}$ period, and it coincides with the 80-s period over which we measured L_{eff}. In the human subject experiment, we used 512 points for the FFT because the breathing frequency was lower (0.22–0.26 Hz) than that of the piglets

(0.6–0.9 Hz) and we wanted to have a similar number of breathing periods. As in the piglets experiment, we averaged the results from multiple (500–1,000) successive FFTs.

The spectrum of the amplitude of the absorption oscillations at the respiratory frequency $[\Delta\mu_a^{resp}(\lambda_i)]$ was fitted with a linear combination of the HbO_2 and Hb extinction spectra, $\varepsilon_{HbO_2}(\lambda_i)\Delta[HbO_2]^{resp} + \varepsilon_{Hb}(\lambda_i)\Delta[Hb]^{resp}$, where $\varepsilon_{HbO_2}(\lambda_i)$ and $\varepsilon_{Hb}(\lambda_i)$ are the extinction coefficients of HbO_2 and Hb, respectively (43, 53). The fitting parameters were the amplitudes of the oscillatory concentration of oxyhemoglobin ($\Delta[HbO_2]^{resp}$) and deoxyhemoglobin ($\Delta[Hb]^{resp}$) at the respiratory frequency. The minimization of the sum of the squares of the residuals, i.e., $\sum_i[\Delta\mu_a^{fit}(\lambda_i) - \Delta\mu_a^{resp}(\lambda_i)]^2$, yields a linear system whose solution gives the following best fit concentrations of amplitude of the oscillatory $[HbO_2]$ and $[Hb]$ (11)

$$\Delta[HbO_2]^{resp} = \frac{\begin{aligned}&[\sum_i \Delta\mu_a^{resp}(\lambda_i)\varepsilon_{HbO_2}(\lambda_i)][\sum_i \varepsilon_{Hb}^2(\lambda_i)]\\&- [\sum_i \Delta\mu_a^{resp}(\lambda_i)\varepsilon_{Hb}(\lambda_i)][\sum_i \varepsilon_{HbO_2}(\lambda_i)\varepsilon_{Hb}(\lambda_i)]\end{aligned}}{[\sum_i \varepsilon_{HbO_2}^2(\lambda_i)][\sum_i \varepsilon_{Hb}^2(\lambda_i)] - [\sum_i \varepsilon_{HbO_2}(\lambda_i)\varepsilon_{Hb}(\lambda_i)]^2}$$

$$(3)$$

$$\Delta[Hb]^{resp} = \frac{\begin{aligned}&[\sum_i \Delta\mu_a^{resp}(\lambda_i)\varepsilon_{Hb}(\lambda_i)][\sum_i \varepsilon_{HbO_2}^2(\lambda_i)]\\&- [\sum_i \Delta\mu_a^{resp}(\lambda_i)\varepsilon_{HbO_2}(\lambda_i)][\sum_i \varepsilon_{HbO_2}(\lambda_i)\varepsilon_{Hb}(\lambda_i)]\end{aligned}}{[\sum_i \varepsilon_{HbO_2}^2(\lambda_i)][\sum_i \varepsilon_{Hb}^2(\lambda_i)] - [\sum_i \varepsilon_{HbO_2}(\lambda_i)\varepsilon_{Hb}(\lambda_i)]^2}$$

$$(4)$$

The oxygen saturation of the hemoglobin compartment oscillating synchronously with respiration (Sv_{O_2}-$NIRS_{resp}$) is then given by

$$Sv_{O_2} - NIRS_{resp} = \frac{\Delta[HbO_2]^{resp}}{\Delta[HbO_2]^{resp} + \Delta[Hb]^{resp}}$$

$$= \frac{\begin{aligned}&[\sum_i \Delta\mu_a^{resp}(\lambda_i)\varepsilon_{HbO_2}(\lambda_i)][\sum_i \varepsilon_{Hb}^2(\lambda_i)]\\&- [\sum_i \Delta\mu_a^{resp}(\lambda_i)\varepsilon_{Hb}(\lambda_i)][\sum_i \varepsilon_{HbO_2}(\lambda_i)\varepsilon_{Hb}(\lambda_i)]\end{aligned}}{\begin{aligned}&[\sum_i \Delta\mu_a^{resp}(\lambda_i)\varepsilon_{HbO_2}(\lambda_i)]\{\sum_i \varepsilon_{Hb}(\lambda_i)[\varepsilon_{Hb}(\lambda_i) - \varepsilon_{HbO_2}(\lambda_i)]\}\\&- [\sum_i \Delta\mu_a^{resp}(\lambda_i)\varepsilon_{Hb}(\lambda_i)]\{\sum_i \varepsilon_{HbO_2}(\lambda_i)[\varepsilon_{Hb}(\lambda_i) - \varepsilon_{HbO_2}(\lambda_i)]\}\end{aligned}}$$

$$(5)$$

It is important to note that for the determination of Sv_{O_2}-$NIRS_{resp}$ one only needs to know L_{eff} to within a wavelength-independent factor. In fact, *Eq. 5* shows that a common, wavelength-independent multiplicative factor in $\Delta\mu_a(\lambda_i)$ cancels out in the expression for Sv_{O_2}-$NIRS_{resp}$. In contrast, the wavelength dependence of L_{eff} is important for the measurement of Sv_{O_2} with our method, and this is why we have opted to measure L_{eff} at each wavelength using the multidistance, frequency-domain technique. It is also important to observe that our method requires *1*) oscillations of μ_a at the respiratory frequency to be reliably attributed to hemoglobin (and not, for instance, to motion artifacts), *2*) the hemoglobin concentration fluctuations to result from the volume oscillation of a hemoglobin compartment rather than from periodic fluctuations in the blood flow, and *3*) the fluctuating hemoglobin compartment responsible for the measured $\Delta\mu_a$ to be mainly the venous compartment. In our measurements, we have considered each one of the three above points. The assignment of the absorption oscillations to hemoglobin (*point 1*) was done by requiring that the hemoglobin spectrum fits the absorption data relatively well. To this aim, we requested that the average absolute value of the relative residuals, defined as $\varepsilon^{fit} = 1/N\sum_{i=1}^N |\Delta\mu_a^{fit}(\lambda_i) - \Delta\mu_a^{resp}(\lambda_i)|/\Delta\mu_a^{fit}(\lambda_i)$, where N is the number of wavelengths considered, be at most twice the experimental percent error in $\Delta\mu_a^{resp}$. We also used the standard deviation of the Sv_{O_2}-$NIRS_{resp}$(FFT) values obtained with the 800 (piglet experiment) or 500–1,000 (human experiment) successive FFTs to estimate the

error in Sv_{O_2}-$NIRS_{resp}$(FFT). We discarded the cases having a standard deviation error in Sv_{O_2}-$NIRS_{resp}$ greater than 15%. The assignment of the absorption oscillations to volume rather than blood flow fluctuations (*point 2*) is achieved by verifying that the absorption oscillations at the eight wavelengths are in phase. In fact, blood flow fluctuations induce out-of-phase oscillations in the [HbO_2] and [Hb] (because of the increased rates of inflow of HbO_2 and washout of Hb), as opposed to the in-phase oscillations of HbO_2 and Hb that result from volume pulsations. The third point, namely the requirement that the absorption oscillations at the respiratory frequency are representative of venous blood, is investigated by *1*) comparing the Sv_{O_2}-NIRS from the respiratory hemoglobin oscillations (Sv_{O_2}-$NIRS_{resp}$) with the corresponding values measured by gas analysis of Sv_{O_2}-blood (piglet experiments) or by the NIRS venous occlusion method (Sv_{O_2}-$NIRS_{vo}$) (human subject experiments), *2*) studying the effect on the [Hb] and [HbO_2] oscillations at the respiratory frequency of a venous occlusion induced between the lungs and the peripheral measurement area (the thigh muscles in human subject experiments), and *3*) by recording the effect of muscle exercise on the near-infrared measurements of Sv_{O_2} [Sv_{O_2}-$NIRS_{resp}$(BP)] in human subjects.

RESULTS

Figure 4 reports average spectra of L_{eff} measured for a source-detector separation of 1 cm. Figure 4*A* refers to piglet measurements conducted at two different values of $F_{I_{O_2}}$, whereas Fig. 4*B* refers to human measurements with *probes HVM* and *HVL*. The error bars in
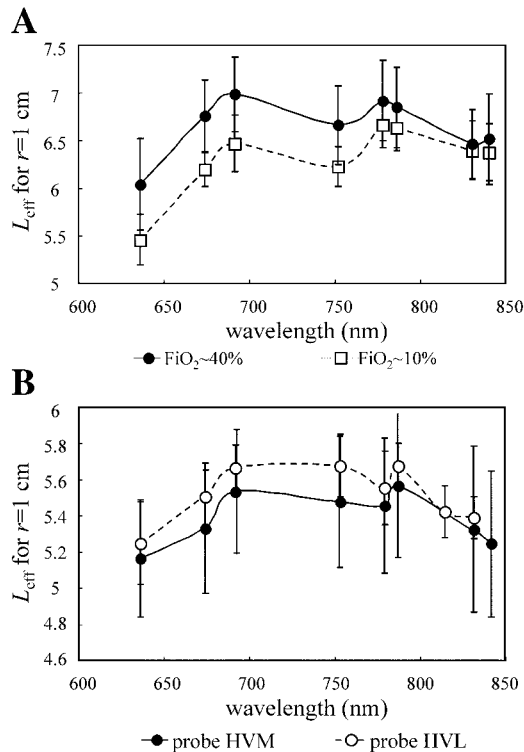

Fig. 4. Near-infrared spectra of the effective optical pathlength (L_{eff}) measured on the piglet's leg (*A*) and a human thigh muscle (*B*) for a source-detector separation (*r*) of 1 cm. In *A*, different symbols refer to 2 different values of $F_{I_{O_2}}$. In *B*, different symbols refer to 2 different thigh muscles (vastus medialis for *probe HVM* and vastus lateralis for *probe HVL*). The lines join the points as an aid to the eye.

Fig. 4 represent the standard deviations over multiple measurements (multiple $F_{I_{O_2}}$ cycles and piglets for Fig. 4*A* and multiple subjects for Fig. 4*B*).

In the piglet experiment, we discarded 11 (from a total of 67) Sv_{O_2}-$NIRS_{resp}$(FFT) measurements because the standard deviation over 800 FFTs exceeded 15%. These discarded Sv_{O_2}-$NIRS_{resp}$(FFT) readings occurred as follows: one (of 8) in *piglet 1*, two (of 26) in *piglet 2*, and eight (of 33) in *piglet 3*. One discarded reading was assigned to motion artifacts, whereas the other ten discarded measurements all occurred at low-$F_{I_{O_2}}$ values (10–17.5%) corresponding to Sv_{O_2}-blood values of 20–50%. We were not able to apply the BP method to *piglet 2* and to the $F_{I_{O_2}}$ *cycles A* and *B* of *piglet 3* because of irregular absorption oscillation waveforms that were not reliably processed by the BP + MA approach.

Figure 5 shows typical temporal traces of the relative [HbO_2] and [Hb] measured on the piglet's leg (with optical *probe PR*) (Fig. 5*A*) and on the human vastus medialis muscle at rest (Fig. 5*B*) and during venous occlusion on the upper thigh (optical *probe HVM*) (Fig. 5*C*). The temporal traces of [Hb] and [HbO_2] are obtained by fitting the measured spectrum of $\Delta\mu_a(\lambda,t)$ (whose value at each wavelength was obtained from *Eq. 2*) with a linear combination of the HbO_2 and Hb extinction spectra. This procedure results in the application of *Eqs. 3* and *4* without the superscript "resp" on $\Delta\mu_a$, Δ[HbO_2], and Δ[Hb]. Two oscillatory components are clearly visible in the relative [HbO_2] and [Hb] traces of Fig. 5*A*: the first one, associated with the heartbeat (as shown by the pulse oximeter data; top trace in Fig. 5) is at a frequency of ~2.5 Hz, whereas the second one, associated with respiration (as shown by the strain gauge signal; second trace from the top in Fig. 5), is at a frequency of ~0.65 Hz. Only the latter oscillatory component (at a frequency of ~0.23 Hz in human subjects) is clearly visible in Fig. 5*B*, whereas neither is present in Fig. 5*C*. Figure 5, *B* and *C*, shows additional low-frequency oscillations associated with changes in blood pressure and heart rate. We observe that the strain-gauge signal (second trace from the top in Fig. 5) increases during inspiration and decreases during expiration. The BP filter described in the previous section aims at isolating the oscillatory component at the respiratory frequency by filtering out higher and lower frequency components. The relative [HbO_2] and [Hb] traces after BP filtering are shown in Fig. 5, *bottom*. In the case reported in Fig. 5, which is representative of the results reported in this article for Sv_{O_2}-$NIRS_{resp}$, the oscillatory components of [HbO_2] and [Hb] at the respiratory frequency are in phase with each other and disappear during venous occlusion.

Figure 6 illustrates representative $\Delta\mu_a^{resp}$ spectra measured on the piglet's leg (*probe PR*) (Fig. 6*A*) and on the human vastus medialis muscle at rest (Fig. 6*B*) and during venous occlusion on the upper thigh (*probe HVM*) (Fig. 6*C*). The *y*-axis of each panel of Fig. 6 refers to the values of $\Delta\mu_a^{resp}$ obtained with the BP filter method. The values of $\Delta\mu_a^{resp}$ computed with the FFT method are normalized by a wavelength-independent
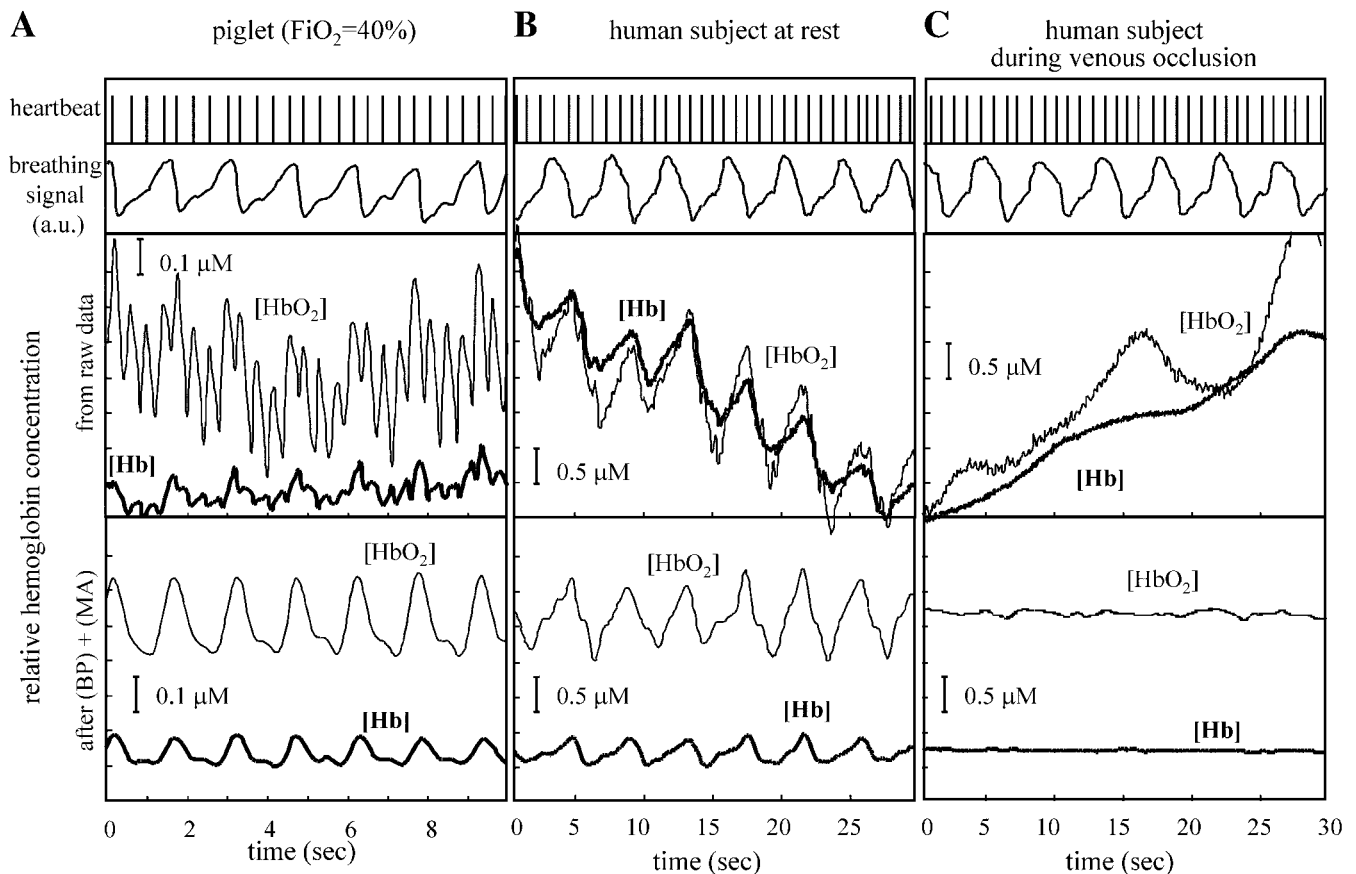
Fig. 5. Representative traces of the relative HbO₂ concentrations ([HbO₂]) and Hb concentrations ([Hb]) measured on the piglet's leg (with optical *probe PR*) (*A*) and on the human vastus medialis muscle at rest (*B*) and during venous occlusion on the upper thigh (optical *probe HVM*) (*C*). *Bottom panels* report the [Hb] traces after processing with the digital band-pass filter [band pass (BP) + modeling algorithm (MA)] designed to isolate the oscillations at the respiratory frequency. *Top trace* represents the piglet's heartbeat monitored by the pulse oximeter. *Second trace* from the top is the strain gauge signal that monitors the respiratory excursion. The strain gauge signal increases during inspiration and decreases during expiration. a.u., Arbitrary units.

factor to match the BP value of $\Delta\mu_a^{resp}$ at 636 nm. The relatively high value of ϵ^{fit} during venous occlusion (Fig. 6*C*) is an indication of the poor fit, which in turn results from the lack of hemoglobin oscillations at the respiratory frequency (see Fig. 5*C*, *bottom*, and the *y*-axis values of Fig. 5*C* compared with those of Fig. 5*B*). Figure 6 also shows the best fit of the hemoglobin absorption spectrum to the BP $\Delta\mu_a^{resp}$ and to the FFT $\Delta\mu_a^{resp}$. The best-fit hemoglobin spectra represent the oxygen saturation of hemoglobin, as illustrated in Fig. 1. The value of Sv_{O_2}-NIRS$_{resp}$ is given by *Eq. 5*.

Figure 7 compares the measurements of Sv_{O_2}-NIRS$_{resp}$(BP), Sv_{O_2}-NIRS$_{resp}$(FFT), and Sv_{O_2}-blood during *cycle A* of *piglet 1* and during *cycle C* of *piglet 3*. The Sv_{O_2}-NIRS$_{resp}$(BP) traces reported in Fig. 7 were obtained by performing a running average of the breath-to-breath values obtained with the BP method. In Fig. 7, the averaging procedure consists of a 5-point (in Fig. 7*A*) or 15-point (in Fig. 7*B*) running average. The assessment of the agreement between the measurements of Sv_{O_2}-NIRS$_{resp}$(FFT) and Sv_{O_2}-blood in the full piglet study is carried out according to the procedure described by Bland and Altman (5). Figure 8*A* plots the

results of the NIRS method based on the respiratory oscillations of the tissue absorption against the invasive measurement of Sv_{O_2}-blood. The shape of the symbols in Fig. 8*A* indicates the piglet number, whereas the type of fill indicates the location of the NIRS measurement. The range of Sv_{O_2}-blood values considered in this study is ~20–95%. The error bars in Fig. 8*A* are the standard deviations (SD) computed from the results of ~800 successive FFTs (as described in MATERIALS AND METHODS). Figure 8*B* displays the difference between the two readings vs. their average, and it quantifies the discrepancy between the two methods and the possible dependence of such a difference on the level of Sv_{O_2}. The mean difference between Sv_{O_2}-NIRS$_{resp}$ and Sv_{O_2}-blood over the full oxygenation range considered in this study is 1.0% (a measurement of the bias of the Sv_{O_2}-NIRS$_{resp}$ measurement), and the SD of the difference is 5.8%. Figure 8*B* does not show any striking dependence of the difference on the mean. If we take the values of mean difference ± 2 SD as the limits of agreement of the two methods (5), we get an estimate of the maximal discrepancies between Sv_{O_2}-NIRS$_{resp}$(FFT) and Sv_{O_2}-blood of −10.6% and +12.6%.

A

piglet (FiO_2=40%)

$\varepsilon^{(fit)}_{(BP)} = \varepsilon^{(fit)}_{(FFT)} = 6\%$

B

human subject at rest

$\varepsilon^{(fit)}_{(BP)} = \varepsilon^{(fit)}_{(FFT)} = 4\%$

C

human subject during venous occlusion

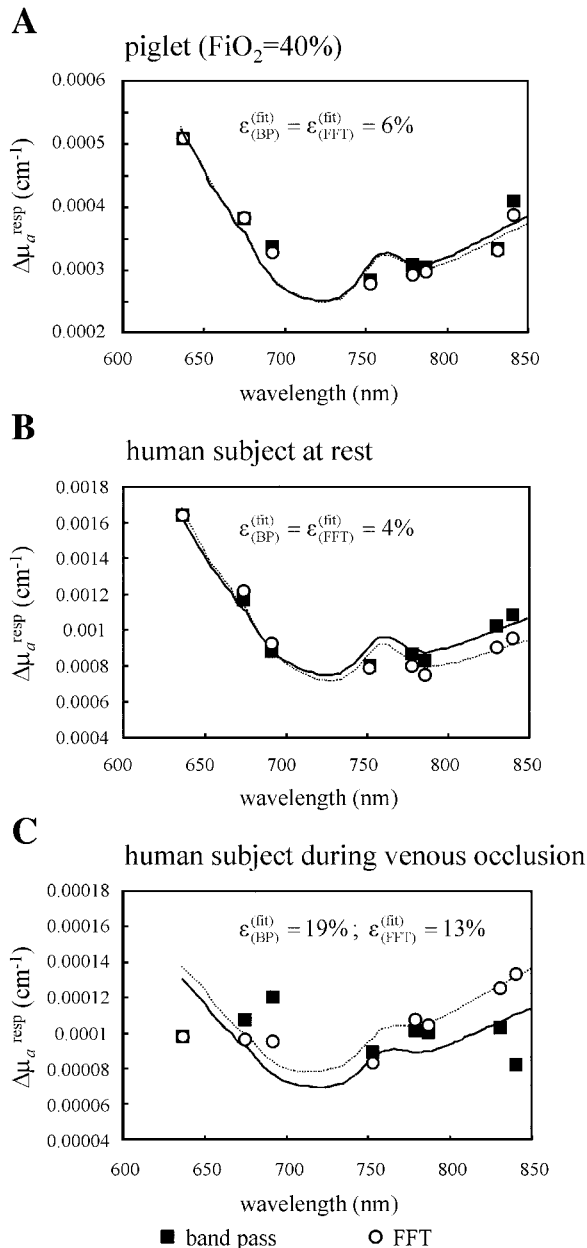$\varepsilon^{(fit)}_{(BP)} = 19\%$; $\varepsilon^{(fit)}_{(FFT)} = 13\%$

■ band pass　　○ FFT

Fig. 6. Representative change in respiratory tissue absorption coefficient ($\Delta\mu_a^{resp}$) spectra measured with the BP and fast Fourier transform (FFT) methods on the piglet's leg (*probe PR*) (*A*) and on the human vastus medialis muscle at rest (*B*) and during venous occlusion on the upper thigh (*probe HVM*) (*C*). The experimental 8-point $\Delta\mu_a^{resp}$ spectra were fitted with the hemoglobin absorption spectrum (with the oxy- and deoxyhemoglobin concentrations as fitting parameters). The values of ε^{fit} (defined in the text) for the BP and FFT spectra give a measure of the quality of the fit.

In the human experiment, we found that the NIRS values of Sv_{O_2} measured with *probe HVM* (placed on top of a visible vein) were typically smaller than those measured with *probe HVL* (placed far from any visible vein). Furthermore, the amplitude of the oscillatory absorption at the respiration (heartbeat) frequency was typically greater (smaller) for the data collected with *probe HVM* than with *probe HVL*. Of the 16 Sv_{O_2}-NIRS$_{resp}$ measurements (8 subjects, 2 locations),

we discarded only 2 measurements (because of a value of Σ^{fit} greater than twice the error in $\Delta\mu_a^{resp}$), both collected with *probe HVL*. Figure 9 compares the Sv_{O_2}-NIRS$_{resp}$ values measured in the human subjects at rest in which the FFT method and the BP filtering approach were used. Figure 9*A* shows the good agreement of the two measurements, and Fig. 9*B* quantifies the average difference (0.9%) and the maximum discrepancies of -5.1 and $+6.9\%$, as given by the mean $\pm$ 2 SD of the differences. Figure 10 reports a similar comparison between Sv_{O_2}-NIRS$_{resp}$(FFT) and Sv_{O_2}-NIRS$_{vo}$. As described by Yoxall and Weindling (56), under the assumption that a venous occlusion induces an initial increase in the venous blood volume, Sv_{O_2}-NIRS$_{vo}$ is given by $[\dot{Hb}O_2]_0/[\dot{Hb}-T]_0$, where the dots indicate a time derivative and the subscript 0 indicates the initial time that immediately follows the onset of venous occlusion. The agreement between Sv_{O_2}-NIRS$_{resp}$(FFT) and Sv_{O_2}-NIRS$_{vo}$ is good, with an average deviation of 0.8% and maximum discrepancies of -4.2 and $+5.8\%$. Two horizontal lines in Figs. 8*B* and 9*B* indicate the range given by the mean difference $\pm$ 2 SD. The maximum discrepancy among Sv_{O_2}-NIRS$_{resp}$-(FFT), Sv_{O_2}-NIRS$_{resp}$(BP), and Sv_{O_2}-NIRS$_{vo}$ is less than the maximum deviation between Sv_{O_2}-NIRS$_{resp}$(FFT) and Sv_{O_2}-blood found in piglets (see Fig. 8*B*).

The effect of muscle exercise on the measurement of Sv_{O_2}-NIRS$_{resp}$(BP) on top of a visible superficial vein (*probe HVM*) is illustrated in Fig. 11. Although Sa_{O_2} (measured with a pulse oximeter) is unaffected by the exercise, Sv_{O_2}-NIRS$_{resp}$(BP) shows a significant postexercise decrease from a baseline value of 75–78% down to a minimum value of ~54%. The recovery to the baseline value of Sv_{O_2}-NIRS$_{resp}$(BP) occurs after ~30 s. By using the BP approach, we could monitor Sv_{O_2}-NIRS$_{resp}$ at every breathing period, i.e., every ~5 s, thus achieving a real-time monitoring of Sv_{O_2}. We observe that we could not obtain meaningful measurements of Sv_{O_2}-NIRS$_{resp}$ during exercise because of motion artifacts.

DISCUSSION

Various methods for measuring Sv_{O_2}. The method presented in this article to measure Sv_{O_2} from the near-infrared absorption oscillations at the respiratory frequency (spiroximetry) can be implemented by using a FFT or a digital BP filter in conjunction with a MA. We have indicated the measurements of Sv_{O_2} obtained with these two approaches with the notations Sv_{O_2}-NIRS$_{resp}$(FFT) and Sv_{O_2}-NIRS$_{resp}$(BP), respectively. An alternative method for measuring Sv_{O_2} with NIRS is based on a previously described venous occlusion protocol (13, 39, 55, 56). We have identified the results of this measurement procedure with the notation Sv_{O_2}-NIRS$_{vo}$. In the human study, the NIRS measurements were conducted at two locations on the thigh. One location was on top of a visible superficial vein of the vastus medialis muscle (*probe HVM*), and the second location was far from visible superficial veins on the vastus lateralis muscle (*probe HVL*). Finally, the inva-

Fig. 7. Comparison between the continuous measurement of Sv_{O_2}-$NIRS_{resp}$ (BP) and the discontinuous measurements of Sv_{O_2}-$NIRS_{resp}$(FFT) and Sv_{O_2}-blood. *A* refers to *cycle A of piglet 1*, whereas *B* refers to *cycle C of piglet 3*. The values of FI_{O_2} (%, left *y*-axes) during the experiment are indicated by the shaded profiles.
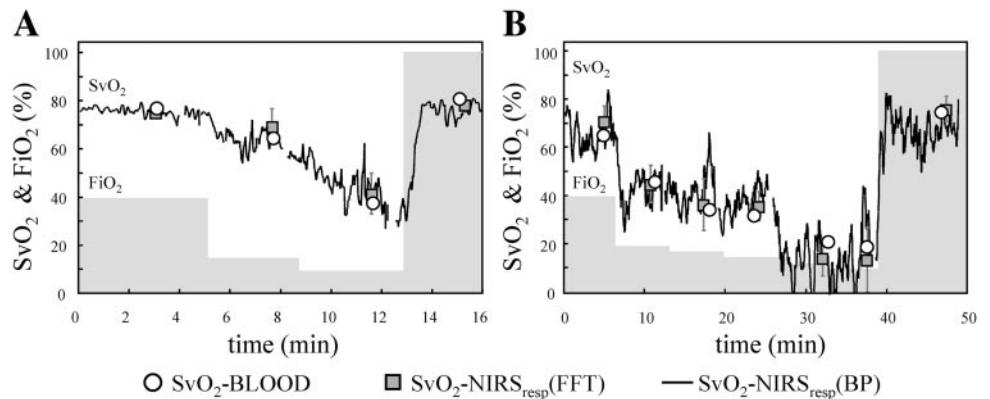
sive measurement of Sv_{O_2} performed by the gas analysis of venous blood samples is indicated with Sv_{O_2}-blood. In this section, we discuss the different features of these measurements of Sv_{O_2}, and the comparison of their results, as reported in Figs. 7–9.

The FFT and BP filter approaches to near-infrared spiroximetry. The major advantage of the BP approach is that it allows for a real-time measurement of Sv_{O_2} by providing a reading of Sv_{O_2}-$NIRS_{resp}$(BP) at every respiration cycle. Consequently, this method is particularly effective during transients, as illustrated by the recovery of the Sv_{O_2}-$NIRS_{resp}$(BP) traces corresponding to the sudden increase of FI_{O_2} to 100% in piglets (see Fig. 6, *A* and *B*), or to the end of the exercise period in human subjects (see Fig. 11). On the other hand, the BP filter + MA method is susceptible to fluctuations in the respiratory frequency and to irregular respiration patterns. This accounts for the fact that we did not get reliable readings of Sv_{O_2}-$NIRS_{resp}$(BP) in *piglet 2* and in FI_{O_2} *cycles A* and *B* of *piglet 3*. The FFT method was more robust, producing reliable readings in 56 of 67 cases (84%) in the piglet study and in 14 of 16 cases (87%) in the human study. It is important to observe that 10 of the 11 discarded readings in piglets occurred at low-Sv_{O_2}-NIRS-blood values (20–50%), and one was

assigned to motion artifacts. Both discarded readings in the human study were collected with *probe HVL*, which was placed far from visible veins. Therefore, we have found indications that the measurement of Sv_{O_2}-$NIRS_{resp}$(FFT) is particularly robust at Sv_{O_2} values >50% (in piglets) and when the optical probe is placed on top of a visible superficial vein (in human subjects). Although the FFT method, which is based on a measurement of the integrated peak at the respiratory frequency, is less sensitive than the BP method to irregular respiration patterns, it is not applicable during transients. In fact, we did not obtain reliable readings of Sv_{O_2} when the time frame used to compute Sv_{O_2}-$NIRS_{resp}$(FFT) (80 s in piglets, 80–120 s in human subjects) included significant changes in the Sv_{O_2}. When both the FFT and the BP methods can be applied, they provide Sv_{O_2}-$NIRS_{resp}$ measurements that are in excellent agreement, as shown in Figs. 6 and 9. The differences between the two measurements (SD of 3.0%) are comparable with measurement errors and significantly less than the maximum deviation between Sv_{O_2}-$NIRS_{resp}$(FFT) and Sv_{O_2}-blood (approximately ±10%) observed in the piglet study (see Fig. 8*B*).

Fig. 8. Comparison of Sv_{O_2}-$NIRS_{resp}$ (FFT) and Sv_{O_2}-blood in the piglet study. The shape of the symbols refer to the piglet (circles, *piglet 1*; squares, *piglet 2*; triangles, *piglet 3*), whereas the filling indicates the measurement side (filled symbols, right leg, i.e., *probe PR*; open symbols, left leg, i.e., *probe PL*). *A*: Sv_{O_2}-$NIRS_{resp}$(FFT) is plotted vs. Sv_{O_2}-blood. *B*: difference is plotted vs. the average of the 2 measurements. Two horizontal lines indicate the range given by mean difference ± 2 SD (SD is the standard deviation of the difference between the 2 measurements).
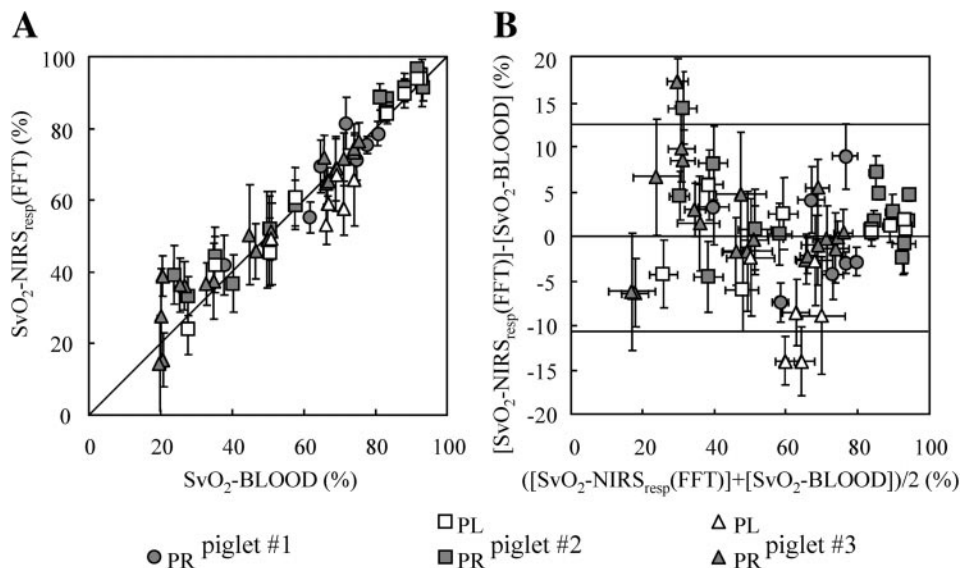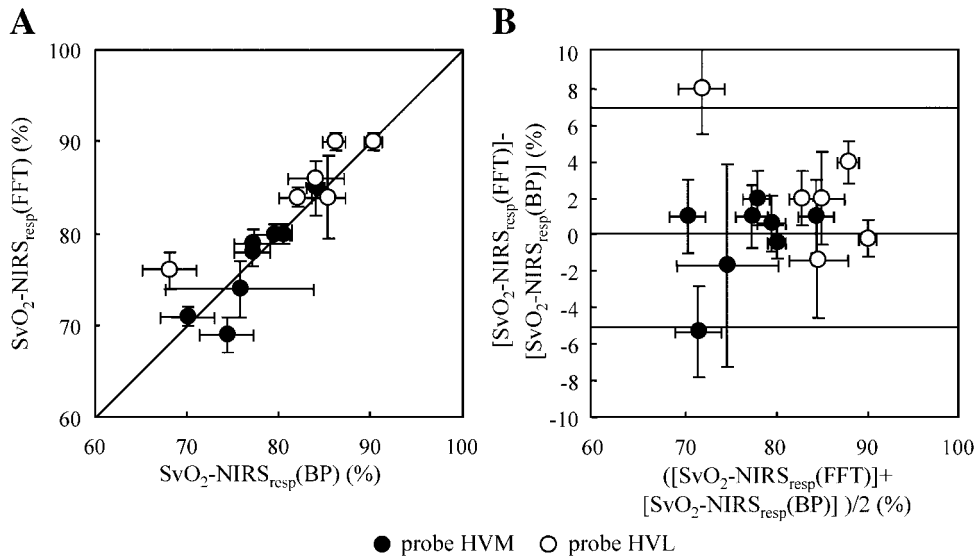
Fig. 9. Comparison of Sv_{O_2}-$NIRS_{resp}$ (FFT) and Sv_{O_2}-$NIRS_{resp}$(BP) in the human study. ●, Vastus medialis muscle; i.e., *probe HVM*. ○, Vastus lateralis muscle; i.e., *probe HVL*. *Probe HVM* was place on top of a visible superficial vein, whereas *probe HVL* was far from visible veins. *A*: Sv_{O_2}-$NIRS_{resp}$(FFT) is plotted vs. Sv_{O_2}-$NIRS_{resp}$(BP). *B*: difference is plotted vs. the average of the 2 measurements. Two horizontal lines in *B* indicate the range given by mean difference ± 2 SD.

Measurements of Sv_{O_2}-$NIRS_{resp}$ and Sv_{O_2}-$NIRS_{vo}$. Both of these NIRS methods to measure the Sv_{O_2} (resp and vo) rely on a change in the volume fraction of venous blood in the tissue. The two major differences between the two methods are as follows. *1*) The vo method requires an external perturbation consisting of a pneumatic-cuff-induced venous occlusion, whereas the resp method is only based on the intrinsic blood pressure oscillations induced by normal respiration and can be applied continuously. *2*) The vo method can be applied only to limbs, whereas the resp method can, in principle, be applied to any tissue and in particular to the brain, as already shown by Wolf et al. (52). However, we stress that it is always important to verify that the [HbO_2] and [Hb] oscillate in phase at the respiratory frequency for the resp method to provide reliable measurements of Sv_{O_2}. For instance, Elwell et al. (16) reported out-of-phase oscillations of [Hb] and [HbO_2] in the human brain, which would indicate a blood

flow rather than volume oscillations, thus rendering the resp method inapplicable. In our human study, we found an excellent agreement between Sv_{O_2}-$NIRS_{resp}$(FFT) and Sv_{O_2}-$NIRS_{vo}$, with a maximum deviation on the order of ±4–5% (see Fig. 10).

Optical probes PR, PL, HVM, and HVL. In the piglet study, we have found no significant difference between the Sv_{O_2}-$NIRS_{resp}$(FFT) data collected with *probes PR* (on the right leg) and *PL* (on the left leg, where the venous catheter was inserted) (see Fig. 8*A*). This result indicates that noninvasive measurements of Sv_{O_2} on one leg can be meaningfully compared with invasive measurements of Sv_{O_2} on the other leg. In the human study, we found some differences between the Sv_{O_2}-NIRS measurements with *probe HVM* (placed on top of a visible superficial vein in the vastus medialis muscle) and with *probe HVL* (placed far from visible veins on the vastus lateralis muscle). As shown in Figs. 8 and 9, the Sv_{O_2}-NIRS readings (with both the $NIRS_{resp}$ and $NIRS_{vo}$
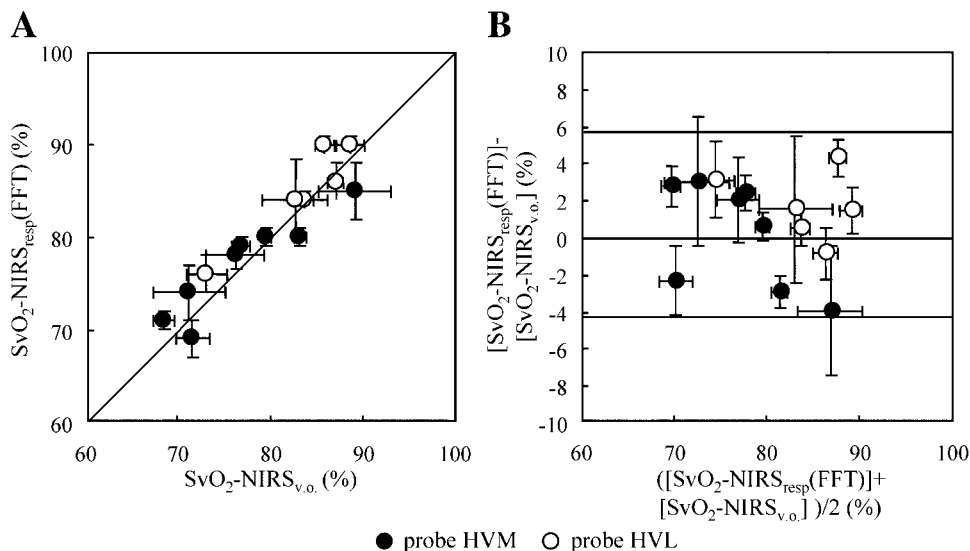

Fig. 10. Comparison of Sv_{O_2}-$NIRS_{resp}$ (FFT) and Sv_{O_2}-$NIRS_{vo}$ (venous occlusion) in the human study. ●, Vastus medialis muscle; i.e., *probe HVM*. ○, Vastus lateralis muscle; i.e., *probe HVL*. *Probe HVM* was place on top of a visible superficial vein, whereas *probe HVL* was far from visible veins. *A*: Sv_{O_2}-$NIRS_{resp}$(FFT) is plotted vs. Sv_{O_2}-$NIRS_{vo}$. *B*: difference is plotted vs. the average of the 2 measurements. Two horizontal lines in *B* indicate the range given by mean difference ± 2 SD.
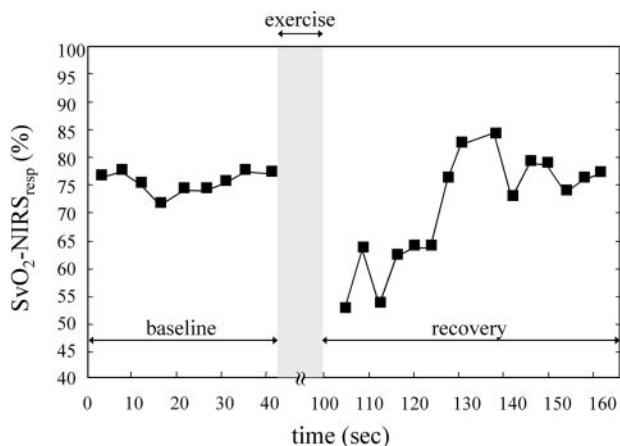
Fig. 11. Continuous measurement of Sv_{O_2}-$NIRS_{resp}$(BP) with optical *probe HVM* (vastus medialis muscle, on top of a visible superficial vein) on a healthy human subject during baseline and after isometric muscle exercise (recovery).

method) of *probe HVM* (see Figs. 8 and 9) were typically smaller than the readings of *probe HVL* (see Figs. 8 and 9). We assign this result to a partial contribution from the capillary and/or arterial compartments picked up by *probe HVL*. In fact, although the optical data from probe HVM shown in Fig. 4, *B* and *C*, do not show any visible contribution from the arterial pulsation, data from *probe HVL* (not shown) do contain pulsatile components at the heartbeat frequency. As a result, we believe that the optical probe should be placed on top of visible superficial veins for more accurate readings of Sv_{O_2}-$NIRS_{resp}$ on human subjects. We believe that the reason that Sv_{O_2}-$NIRS_{resp}$ readings in the piglet study were in close agreement with the invasive measurement of Sv_{O_2}, despite the evident arterial pulsation in Fig. 5*A*, is related to the smaller extent of respiratory sinus arrhythmia in piglets with respect to humans. In fact, respiratory sinus arrhythmia is the main origin of the arterial oscillations at the respiratory frequency (38). The larger role played by respiratory sinus arrhythmia in human subjects with respect to piglets will probably require a more careful interpretation of the optical data for spiroximetry. However, the results of Fig. 11 show the practical applicability of spiroximetry to human subjects, so that we do not expect respiratory sinus arrhythmia to introduce an intrinsic limitation of the method.

Noninvasive vs. invasive measurements of Sv_{O_2}. The comparison between Sv_{O_2}-$NIRS_{resp}$(FFT) and Sv_{O_2}-blood in the piglet study shows a maximum deviation range of -10.6% to $+12.6\%$. The local character of the Sv_{O_2} (as opposed to the systemic nature of the Sa_{O_2}) requires some caution in the comparison of invasive (Sv_{O_2}-blood) and noninvasive (Sv_{O_2}-NIRS) measurements of Sv_{O_2}. In fact, in our piglet study, Sv_{O_2}-blood was measured from blood samples drawn from the femoral vein, whereas Sv_{O_2}-$NIRS_{resp}$ was measured with an optical probe placed on the leg muscle. It is likely that the NIRS oscillatory signal

(at the respiratory frequency) is not just representative of the femoral vein and may therefore be indicative of the oxygen consumption at different tissue areas than those affecting the femoral vein saturation. This fact may not lead to significant differences under rest conditions, but it may be important under stress. Although we found a good agreement between Sv_{O_2}-$NIRS_{resp}$(FFT) and Sv_{O_2}-blood over the whole range of $F_{I_{O_2}}$ values considered (see Fig. 8), we observed a meaningfully greater SD of the differences over the $20-55\%$ Sv_{O_2}-blood range (SD = 7.8%) than in the $55-95\%$ range (SD = 3.6%).

Effect of muscle exercise on Sv_{O_2}-$NIRS_{resp}$(BP). The result reported in Fig. 11 serves the purpose of further illustrating the potential of the Sv_{O_2}-$NIRS_{resp}$(BP) measurement approach. In fact, Fig. 11 shows the feasibility of monitoring the Sv_{O_2} in real time on a breath-to-breath basis (one data point every 4–5 s). Furthermore, the baseline Sv_{O_2}-$NIRS_{resp}$(BP) value of 75–78% and the exercise-induced drop indicate the venous origin of the saturation measurement, since the Sa_{O_2} measurement provided by the pulse oximeter stayed constant at $98 \pm 1\%$ for the whole measurement period. On the other hand, Fig. 11 reports only one representative case, and more studies are required to quantify the effect of muscle exercise on the measurement of Sv_{O_2}-$NIRS_{resp}$.

In conclusion, we have presented a noninvasive approach to measure the Sv_{O_2} in tissues from the near-infrared spectrum of the amplitude of respiration-induced absorption oscillations. We have implemented this approach, which we call near-infrared spiroximetry, by processing the optical data with a FFT method or with a digital BP filter in conjunction with a MA. More sophisticated data processing schemes may further improve the effectiveness and the range of applicability of spiroximetry. The Sv_{O_2} measurements reported in this article complement previously demonstrated NIRS measurements of St_{O_2} (8, 27) and Sa_{O_2} (21). Therefore, our results may lead to the design of a noninvasive optical instrument capable of providing simultaneous and real-time measurements of local Sa_{O_2}, St_{O_2}, and Sv_{O_2}.

REFERENCES

1. **Aoyagi T, Kishi M, Yamaguchi K, and Watanabe S.** Improvement of the earpiece oximeter. In: *Abstracts of the Japanese*

Society of Medical Electronics and Biological Engineering, *Tokyo, Japan, 1974*, p. 90–91.

2. **Bank W, Park J, Lech G, and Chance B.** Near-infrared spectroscopy in the diagnosis of mitochondrial disorders. *Biofactors* 7: 243–245, 1998.

3. **Benaron DA, Hintz SR, Villringer A, Boas D, Kleinschmidt A, Frahm J, Hirth C, Obrig H, van Houten JC, Kermit EL, Cheong WF, and Stevenson DK.** Noninvasive functional imaging of human brain using light. *J Cereb Blood Flow Metab* 20: 469–477, 2000.

4. **Berne RM and Levy MN.** *Cardiovascular Physiology* (7th ed.). St. Louis, MO: Mosby Year Book, 1997, p. 196.

5. **Bland JM and Altman DG.** Statistical methods for assessing agreement between two methods of clinical measurement. *Lancet* 1: 307–310, 1986.

6. **Butler JP, Miki H, Suzuki S, and Takishima T.** Step response of lung surface-to-volume ratio by light-scattering stereology. *J Appl Physiol* 67: 1873–1880, 1989.

7. **Casavola C, Paunescu LA, Fantini S, and Gratton E.** Blood flow and oxygen consumption with near-infrared spectroscopy and venous occlusion: spatial maps and the effect of time and pressure of inflation. *J Biomed Opt* 5: 269–276, 2000.

8. **Chance B, Cope M, Gratton E, Ramanujam N, and Tromberg BJ.** Phase measurement of light absorption and scatter in human tissues. *Rev Sci Instrum* 689: 3457–3481, 1998.

9. **Chance B, Dait M, Zhang C, Hamaoka T, and Hagerman F.** Recovery from exercise-induced desaturation in the quadriceps muscle of elite competitive rowers. *Am J Physiol Cell Physiol* 262: C766–C775, 1992.

10. **Colier WN, Quaresima V, Wenzel R, van der Sluijs MC, Oeseburg B, Ferrari M, and Villringer A.** Simultaneous near-infrared spectroscopy monitoring of left and right occipital areas reveals contralateral hemodynamic changes upon hemifield paradigm. *Vision Res* 41: 97–102, 2001.

11. **Cope M.** *The Application of Near-Infrared Spectroscopy to Non-Invasive Monitoring of Cerebral Oxygenation in the Newborn Infant* (PhD thesis). London: Biomedical Optics Research Group, University College, 1991, p. 263–269. [Online] http://www.medphys.ucl.ac.uk/research/borg/homepages/mcope/index.htm [2001, May 10]

12. **De Blasi R, Cope M, Elwell C, Safoue F, and Ferrari M.** Noninvasive measurement of human forearm oxygen consumption by near infrared spectroscopy. *Eur J Appl Physiol* 67: 20–25, 1993.

13. **De Blasi RA, Ferrari M, Natali A, Conti G, Mega A, and Gasparetto A.** Noninvasive measurement of forearm blood flow and oxygen consumption by near-infrared spectroscopy. *J Appl Physiol* 76: 1388–1393, 1994.

14. **Delpy DT, Cope M, van der Zee P, Arridge S, Wray S, and Wyatt JS.** Estimation of optical pathlength through tissue from direct time of flight measurement. *Phys Med Biol* 33: 1433–1442, 1988.

15. **Elwell CE, Matcher SJ, Tyszczuk L, Meek JH, and Delpy DT.** Measurement of cerebral venous saturation in adults using near infrared spectroscopy. *Adv Exp Med Biol* 411: 453–460, 1997.

16. **Elwell CE, Owen-Reece H, Cope M, Edwards AD, Wyatt JS, Reynolds EOR, and Delpy DT.** Measurement of changes in cerebral heamodynamic during inspiration and expiration using near infrared spectroscopy. *Adv Exp Med Biol* 388: 619–626, 1994.

17. **Fantini S, Franceschini MA, Fishkin JB, Barbieri B, and Gratton E.** Quantitative determination of the absorption spectra of chromophores in strongly scattering media: a light-emitting-diode based technique. *Appl Opt* 33: 5204–5213, 1994.

18. **Fantini S, Franceschini MA, and Gratton E.** Effective source term in the diffusion equation for photon transport in turbid media. *Appl Opt* 36: 156–163, 1997.

19. **Fantini S, Franceschini MA, Maier JS, Walker SA, Barbieri B, and Gratton E.** Frequency-domain multichannel optical detector for non-invasive tissue spectroscopy and oximetry. *Opt Eng* 34: 32–42, 1995.

20. **Franceschini MA, Fantini S, Palumbo R, Pasqualini L, Vaudo G, Franceschini E, Gratton E, Palumbo B, Inno-cente S, and Mannarino E.** Quantitative near-infrared spectroscopy on patients with peripheral vascular disease. *Proc SPIE* 3194: 112–115, 1998.

21. **Franceschini MA, Gratton E, and Fantini S.** Non-invasive optical method to measure tissue and arterial saturation: an application to absolute pulse oximetry of the brain. *Opt Lett* 24: 829–831, 1999.

22. **Fantini S, Hueber D, Franceschini MA, Gratton E, Rosenfeld W, Stubblefield PG, Maulik D, and Stankovic MR.** Non-invasive optical monitoring of the newborn piglet brain using continuous-wave and frequency-domain methods. *Phys Med Biol* 44: 1543–1563, 1999.

23. **Franceschini MA, Moesta KT, Fantini S, Gaida G, Gratton E, Jess H, Mantulin WW, Seeber M, Schlag PM, and Kaschke M.** Frequency-domain instrumentation enhances optical mammography: initial clinical results. *Proc Natl Acad Sci USA* 94: 6468–6473, 1997.

24. **Franceschini MA, Toronov V, Filiaci ME, Gratton E, and Fantini S.** On-line optical imaging of the human brain with 160-ms temporal resolution. *Opt Express* 6: 49–57, 2000.

25. **Franceschini MA, Wallace D, Barbieri B, Fantini S, Mantulin WW, Pratesi S, Donzelli GP, and Gratton E.** Optical study of the skeletal muscle during exercise with a second generation frequency-domain tissue oximeter. *Proc SPIE* 2979: 807–814, 1997.

26. **Fung YC.** *Biomechanics—Circulation* (2nd ed.). New York: Springer-Verlag, 1997, p. 243.

27. **Gratton E, Fantini S, Franceschini MA, Gratton G, and Fabiani M.** Measurements of scattering and absorption changes in muscle and brain. *Philos Trans R Soc Lond B Biol Sci* 352: 727–735, 1997.

28. **Grosenick D, Wabnitz H, and Rinneberg H.** Time-resolved imaging of solid phantoms for optical mammography. *Appl Opt* 36: 221–231, 1997.

29. **Hamaoka T, Iwane H, Shimomitsu T, Katsumura T, Murase N, Nishio S, Osada T, Kurosawa Y, and Chance B.** Noninvasive measures of oxidative metabolism on working human muscles by near-infrared spectroscopy. *J Appl Physiol* 81: 1410–1417, 1996.

30. **Hoshi Y and Tamura M.** Near-infrared optical detection of sequential brain activation in the prefrontal cortex during mental tasks. *Neuroimage* 5: 292–297, 1997.

31. **Hueber DM, Franceschini MA, Ma HY, Xu Q, Ballesteros JR, Fantini S, Wallace D, Ntziachristos V, and Chance B.** Non-invasive and quantitative near-infrared hemoglobin spectrometry in the piglet brain during hypoxic stress, using a frequency-domain multi-distance instrument. *Phys Med Biol* 46: 41–62, 2001.

32. **Komiyama T, Shigematsu H, Yasuhara H, and Muto T.** Near-infrared spectroscopy grades the severity of intermittent claudication in diabetics more accurately than ankle pressure measurement. *Br J Surg* 87: 459–466, 2000.

33. **Kooijman HM, Hopman MT, Colier WN, van der Vliet JA, and Oeseburg B.** Near infrared spectroscopy for noninvasive assessment of claudication. *J Surg Res* 72: 1–7, 1997.

34. **Liu H, Boas DA, Zhang Y, Yodh AG, and Chance B.** Determination of optical properties and blood oxygenation in tissue using continuous NIR light. *Phys Med Biol* 40: 1983–1993, 1995.

35. **Meek JH, Elwell CE, Khan MJ, Romaya J, Wyatt JS, Delpy DT, and Zeki S.** Regional changes in cerebral haemodynamics as a result of a visual stimulus measured by near infrared spectroscopy. *Proc R Soc Lond B Biol Sci* 261: 351–356, 1995.

36. **Mendelson Y.** Pulse oximetry: theory and applications for non-invasive monitoring. *Clin Chem* 38: 1601–1607, 1992.

37. **Millikan GA.** The oximeter, an instrument for measuring continuously the oxygen saturation of arterial blood in man. *Rev Sci Instrum* 13: 434–444, 1942.

38. **Mohrman DE and Heller LJ.** *Cardiovascular Physiology* (4th ed.). New York: McGraw-Hill, Health Professions Division, 1997, p. 177.

39. **Nitzan M, Babchenko A, Khanokh B, and Taitelbaum H.** Measurement of oxygen saturation in venous blood by dynamic near infrared spectroscopy. *J Biomed Opt* 5: 155–162, 2000.

40. **Ntziachristos V, Yodh AG, Schnall M, and Chance B.** Concurrent MRI and diffuse optical tomography of breast after indocyanine green enhancement. *Proc Natl Acad Sci USA* 97: 2767–2772, 2000.

41. **Patterson MS, Chance B, and Wilson BC.** Time resolved reflectance and transmittance for the non-invasive measurement of optical properties. *Appl Opt* 28: 2331–2336, 1989.

42. **Pogue BW, Poplack SP, McBride TO, Wells WA, Osterman KS, Osterberg UL, and Paulsen KD.** Quantitative hemoglobin tomography with diffuse near-infrared spectroscopy: pilot results in the breast. *Radiology* 218: 261–266, 2001.

43. **Prahl S.** *Optical Absorption of Hemoglobin.* [Online] Oregon Medical Laser Center http://omlc.ogi.edu/spectra/hemoglobin/index.html [2001, May 10]

44. **Quaresima V and Ferrari M.** Assessment of quadriceps oxygenation in patients with myopathies by near infrared spectroscopy. *Neurology* 51: 1238–1239, 1998.

45. **Sako T, Hamaoka T, Higuchi H, Kurosawa Y, and Katsumura T.** Validity of NIR spectroscopy for quantitatively measuring muscle oxidative metabolic rate in exercise. *J Appl Physiol* 90: 338–344, 2001.

46. **Shah N, Cerussi A, Eker C, Espinoza J, Butler J, Fishkin J, Hornung R, and Tromberg B.** Noninvasive functional optical spectroscopy of human breast tissue. *Proc Natl Acad Sci USA* 98: 4420–4425, 2001.

47. **Skov L, Pryds O, Greisen G, and Lou H.** Estimation of cerebral venous saturation in newborn infants by near infrared spectroscopy. *Pediatr Res* 33: 52–55, 1993.

48. **Topulos GP, Lipsky NR, Lehr JL, Rogers RA, and Butler JP.** Fractional changes in lung capillary blood volume and oxygen saturation during the cardiac cycle in rabbits. *J Appl Physiol* 82: 1668–1676, 1997.

49. **Varela JE, Cohn SM, Giannotti GD, Dolich MO, Ramon H, Wiseberg JA, and McKenney M.** Near-infrared spectroscopy reflects changes in mesenteric and systemic perfusion during abdominal compartment syndrome. *Surgery* 129: 363–370, 2001.

50. **Villringer A and Chance B.** Non-invasive optical spectroscopy and imaging of human brain function. *Trends Neurosci* 20: 435–442, 1997.

51. **Watzman HM, Kurth CD, Montenegro LM, Rome J, Steven JM, and Nicolson SC.** Arterial and venous contributions to near-infrared cerebral oximetry. *Anesthesiology* 93: 947–953, 2000.

52. **Wolf M, Duc G, Keel M, and Niederer P.** Continuous noninvasive measurement of cerebral arterial and venous oxygen saturation at the bedside in mechanically ventilated neonates. *Crit Care Med* 9: 1579–1582, 1997.

53. **Wray S, Cope M, Delpy DT, Wyatt JS, and Reynolds EOR.** Characterization of the near infrared absorption spectra of cytochrome aa_3 and haemoglobin for the non-invasive monitoring of cerebral oxygenation. *Biochim Biophys Acta* 933: 184–192, 1988.

54. **Yoxall CW, Weindling AM, Dawani NH, and Peart I.** Measurement of cerebral venous oxyhemoglobin saturation in children by near-infrared spectroscopy and partial jugular venous occlusion. *Pediatr Res* 38: 319–323, 1995.

55. **Yoxall CW and Weindling AM.** The measurement of peripheral venous oxyhemoglobin saturation in newborn infants by near infrared spectroscopy with venous occlusion. *Pediatr Res* 39: 1103–1106, 1996.

56. **Yoxall CW and Weindling AM.** Measurement of venous oxyhaemoglobin saturation in the adult human forearm by near infrared spectroscopy with venous occlusion. *Med Biol Eng Comput* 35: 331–336, 1997.